RRAS and RRAS2 mutations are oncogenic drivers in lung cancer and are sensitive to the pan-RAS inhibitor RMC-6236

Alexander J. Pfeil[1,2,3,a], Tom Zhang[1,3,a], Ryan Cheng[1,3], Marissa S. Mattar[1], Leo Gili[1], Rachel Lai[1], Inna Khodos[4], Rohan P. Master[1,3], Jenna-Marie Dix[1], Andrea Gazzo[1,5], Kathryn C. Arbour[6], Elisa de Stanchina[4], Christopher A. Febres-Aldana[7], Marc Ladanyi[1,5,#], Soo Ryum Yang[1,*] and Romel Somwar[1,5,*]

[1]Department of Pathology and Laboratory Medicine, Memorial Sloan Kettering Cancer Center, New York, NY, 10065
[2]University of North Carolina School of Medicine, Chapel Hill, NC, 27599
[3]Graduate Medical Education, Memorial Sloan Kettering Cancer Center, New York, NY, 10065
[4]Anti-tumor Core Facility, Memorial Sloan Kettering Cancer Center, New York, NY, 10065
[5]Human Oncology and Pathogenesis Program, Memorial Sloan Kettering Cancer Center, New York, NY, 10065
[6]Thoracic Oncology Service, Department of Medicine, Memorial Sloan Kettering Cancer Center, New York, NY, 10065
[7]Laboratory of Pathology, National Cancer Institute, National Institute of Health, Bethesda, MD, 20892, USA

[a]These authors contributed equally to this manuscript.

*Co-senior authors

[#]**Author for Correspondence: Marc Ladanyi, MD**, Department of Pathology and Laboratory Medicine, Memorial Sloan Kettering Cancer Center, 1275 York Ave, NY, NY, 10065. Email: ladanyim@mskcc.org

ABSTRACT

Introduction: *RRAS* and *RRAS2* encode a subfamily of RAS-like small GTPases that share considerable structural and functional similarities with the well-known family of *RAS* oncogenes, including *KRAS*, *HRAS*, and *NRAS.* Whether *RAS*-like homologous mutations in *RRAS*/*RRAS2* are oncogenic and actionable drivers in lung cancer remains underexplored.

Methods: An institutional cohort of 8,488 non-small cell lung cancer (NSCLC) samples profiled by comprehensive targeted DNA sequencing (MSK-IMPACT) between 2016-2024 was evaluated for *RRAS*/*RRAS2* mutations. Missense mutations in *RRAS*/*RRAS2* homologous to RAS family hotspot mutations were modeled in murine IL3-dependent Ba/F3 cells and immortalized human bronchiolar epithelial cells (HBEC). The oncogenic potential, signaling characteristics, and sensitivity to PI3K and MAPK inhibitors, including the novel pan-RAS inhibitor RMC-6236, were evaluated *in vitro* and *in vivo*.

Results: *RRAS*^{Q87L} or *RRAS2*^{Q72L} variants, homologous to *KRAS*-codon 61 substitutions, were found in ~0.45% of NSCLCs (38/8,488), with all but two lacking other RTK-MAPK oncogenic drivers. RRAS^{Q87L} and RRAS2^{Q72L} mutations were transforming in Ba/F3 and HBEC cells and resulted in strong MAPK and PI3K-mTOR pathway activation. The novel pan-RAS inhibitor RMC-6236 inhibited growth of RRAS^{Q87L} and RRAS2^{Q72L} cell lines and reduced tumor growth *in vivo*. RMC-6236 treatment in *RRAS*^{Q87L} or *RRAS2*^{Q72L} mutant HBECs reduced ERK phosphorylation, induced expression of pro-apoptotic mediators, and inhibited cell cycle progression.

Conclusions: RRAS^{Q87L} and RRAS2^{Q72L} are novel and potentially actionable oncogenic drivers in NSCLC. Our study supports the inclusion of *RRAS/RRAS2* into routine molecular diagnostic panels for precision oncology and provides preclinical rationale for investigating the potential therapeutic utility of pan-RAS inhibitors for patients with RRAS^{Q87L} and RRAS2^{Q72L} lung cancers.

INTRODUCTION

The *RAS* family of small-GTPases are among the most frequently mutated oncogenes in human cancers, present in approximately 10-30% of all tumors.[1,2] These "molecular switches" alternate between their GDP-bound, inactive state and GTP-bound, active state in response to growth factor-receptor-tyrosine kinase (RTK) signaling to regulate cellular growth, proliferation, and survival.[3] Hyperactivation of RAS family members due to genetic mutations is capable of driving tumorigenesis via the RAF/MEK/ERK (MAPK) pathway.[4] The most well-studied RAS isoforms are KRAS, HRAS, and NRAS, all sharing roughly 80% primary amino acid sequence homology.[5] *KRAS* is the most frequently mutated oncogene in most tumor types and is particularly prevalent in colon, lung and pancreatic cancers.[6] In lung adenocarcinoma (LUAD), *KRAS* mutations are seen in up to a third of tumors, with single amino acid substitutions at codons 12, 13 and 61 being the most common hotspots.[7] Small molecule inhibitors of $KRAS^{G12C}$, including sotorasib and adagrasib, have demonstrated clinical efficacy and proof-of-concept for targeting mutant KRAS in multiple cancer types.[8] These therapies, however, are currently restricted to $KRAS^{G12C}$-expressing tumors, which represent only 40% of KRAS mutant NSCLCs and 10-13% of all NSCLCs.[9] The other RAS isoforms are also important drivers of tumorigenesis found in 25% of all RAS-mutant cancers.[2] As such, investigation into targeting additional RAS mutants and inhibitors that target all RAS family members with broader applicability has accelerated, with multiple promising therapies under clinical investigation in recent years.[10]

RRAS and *RRAS2* encode members of a distinct but related subfamily of RAS-like GTPases that share approximately 55% sequence identity with classical RAS isoforms. Although highly conserved in regions involved in guanine nucleotide-binding, GEF/GAP interactions, and effector binding, RRAS and RRAS2 possess unique N- and C-terminal regions that influence subcellular localization and differential activation of downstream effectors. [11] Hence, RRAS proteins are thought to have both overlapping and distinct signaling properties to classic RAS-family proteins, capable of activating RAF, PI3K, and RAL-GEF amongst other effectors, to promote cellular proliferation and survival.[11] RRAS primarily localizes to focal adhesions and is involved in inside-out activation of integrin signaling, contributing to the balance of migration and adhesion signaling.[12] In addition to activating the MAPK pathway, some reports have suggested that RRAS can preferentially signal through the PI3K-AKT pathway in certain cellular contexts.[13,14] For instance, constitutively activated RRAS in breast epithelial cells induced migration through PI3K activation, but not MAPK.[15] RRAS2 is also capable of activating both MAPK and PI3K-AKT signaling, albeit with weaker affinity for RAF-family proteins and subsequently weaker ERK1/2 stimulation than other RAS-family members.[16,17,18] In multiple cell types, RRAS2 has been demonstrated to signal in a MAPK-independent manner, with knockout models of B and T cells resulting in impaired activation of the PI3K-AKT-MTOR pathway. Hence, the primary signaling axis influenced by RRAS and RRAS2 appears to be cell-type and context specific.

Molecular alterations in RRAS and RRAS2 in regions involving guanine nucleotide exchange or intrinsic GTPase activity have been shown to induce transformation *in vitro*.[19-21] Many of these mutations occur at residues homologous to those at KRAS hotspots, primarily at codons 12 and 61, corresponding to codons 38 and 87 in RRAS and 23 and 72 in RRAS2, respectively. Furthermore, ectopic expression of wild-type RRAS2 is capable of transformation in pre-clinical models of triple-negative breast cancer and chronic lymphocytic leukemia.[22-24] Despite homology with common driver genes and oncogenicity *in vitro,* few studies have identified *RRAS* or *RRAS2* mutations in human cancers. *RRAS2* mutations have been identified at high frequencies in KIT^{+} germ cell tumors (11.8%) and central nervous system germinomas

(14.6%).[25,26] *RRAS* family proteins have also been identified in cases of the so-called RASopathies, a family of congenital disorders driven by the dysregulation of RAS signaling, including Noonan Syndrome and associated juvenile myeloid neoplasms.[27,28] Due to the relatively rare occurrence of RRAS and RRAS2 mutations in clinical practice, the relevance and therapeutic implications of these mutations have not been well-studied.

Despite tumor DNA sequencing becoming more accessible with expanding coverage of oncogenes, the prevalence of RRAS family mutations in lung cancers remains poorly characterized, potentially owing to the lack of coverage of *RRAS* and *RRAS2* in most commercial and academic tumor DNA sequencing assays. By leveraging the MSK-IMPACT panel with complete coverage of RRAS and RRAS2, we were able to identify hotspot mutations in LUADs that lacked other known activating alterations in the RTK-RAS-RAF pathway. In this study, we set out to characterize the signaling alterations caused by these mutations and more importantly, if these signaling programs render such tumors susceptible to targeted therapies including the novel and clinically-active pan-RAS inhibitors in trials given the sequence homology between RAS and RRAS/RRAS2.

MATERIAL AND METHODS

Case selection

The study was approved by the Institutional Review Board (IRB) of MSKCC and conducted in accordance with the principles outlined in the Declaration of Helsinki. All patients in this study signed a written informed consent form per the protocol approved by the MSKCC IRB. A retrospective search for *RRAS* and *RRAS2* mutations was performed for NSCLC tissue samples that were genotyped using select MSK-IMPACT panels with full coverage of all *RRAS* (NM_006270) and *RRAS2* (NM_012250) exons, namely the MSK-IMPACT 468 and 505 panels between September 2016 to March 2024. In patients with multiple NSCLCs submitted for sequencing, the genomic profile from the initial tumor or those with *RRAS/RRAS2* mutations were included for analysis.

MSK-IMPACT testing

Genomic DNA from tissue (tumor) and matched blood samples (normal) were extracted for MSK-IMPACT as described previously.[29] In brief, MSK-IMPACT is a hybrid capture-based next-generation sequencing (NGS) assay that interrogates all exons and select introns of cancer-related genes (468 or 505-genes) to identify mutations, copy number alterations, and select structural variants from tumor tissue. Tumor mutation burden (TMB) was calculated by dividing the total number of nonsynonymous somatic mutations (single nucleotide and small insertions/deletions) by the size of the targeted coding regions. All somatic alterations that were (i) annotated as oncogenic and likely oncogenic by OncoKB[30] and/or (ii) present in the cancer hotspot database[31] were classified as driver/pathogenic; all else were considered variants of unknown significance. For all variants outside of *RRAS* and *RRAS2*, only driver alterations were included for analysis.

Clinicopathologic data

Clinical parameters were extracted from the electronic medical records. All tumors underwent central pathologic review for histologic diagnosis according to the 2021 World Health Organization (WHO) classification.[32] For invasive resected lung adenocarcinomas, comprehensive histologic subtyping was performed; using these histologic patterns, IASLC grades were determined.[33]

PD-L1 immunohistochemistry

PD-L1 IHC (E1L3N; dilution 1:100, Cell Signaling Technologies, Danvers, MA) was performed on formalin-fixed paraffin-embedded tissue sections using an automated staining platform (Bond III, Leica). PD-L1 expression was measured using Tumor Proportion Score (TPS) as defined by the percentage of viable tumor cells with partial or complete membranous staining. PD-L1 positivity was defined as having a TPS score of ≥1%.

Reagents and Cell Culture

All cell lines were cultured in a humidified incubator maintained at 5% carbon dioxide at 37°C. The human bronchiolar epithelial cell (HBEC) line was maintained in keratinocyte serum-free media supplemented with 5 ng/mL recombinant EGF and 50 µg/mL bovine pituitary extract (ThermoFisher, Waltham, MA). Untransformed Ba/F3 cells were maintained in RPMI-1640 supplemented with 10% FBS and 5 ng/mL murine IL3 R and D Systems (Minneapolis, MN). Prior to Western blotting experiments, both cell lines were incubated with growth-factor free media for 24 hours prior to sample extraction or treatment. The presence of the mutations of interest within cDNA constructs was confirmed by polymerase chain reaction each time a cell line vial was thawed. Cells were tested for mycoplasma every three months and no cell line was tested positive throughout this study.

RMC-6236 was purchased from STARK Chemicals (New York, NY) and prepared with DMSO for *in vitro* experiments. Primary antibodies used in Western blotting were purchased from Cell Signaling Technologies (Danvers, MA). Secondary anti-mouse or anti-rabbit IgG antibodies conjugated to horseradish peroxide were purchased from R and D Systems (Minneapolis, MN). See **Supplemental Table S1** for details of antibodies used in this study.

cDNA Overexpression of Wild-type and Mutant RRAS and RRAS2

Nucleotides encoding RRAS WT, RRAS Q87L, and RRAS2 WT were ordered as gblocks from Integrated DNA Technologies (Coralville, IA). See **Supplemental Table 2** for exact sequences of gblocks. *RRAS* WT and *RRAS* Q87L sequences were partially codon optimized with no change in predicted amino acid sequence (NM_006270 and its mutated Q87L version), respectively. RRAS2 WT is identical to the coding sequence from the refseq NM_012250. The gblocks and the pCX4 bleo empty vector were digested with AgeI and EcoRI FastDigest enzymes (ThermoFisher, Waltman, MA) for 1 h at 37°C. Bands corresponding to the expected size of the digested products were resolved on 1% (wt/vol) agarose gel at 130 V for 1 h and then extracted using QIAGEN's QIAquick Gel Extraction Kit (Germantown, MD). Assembly of the final plasmids was done utilizing a T4 ligase reaction (ThermoFisher, Waltman, MA) with a 3:1 ratio of insert:backbone. Stable competent E. coli (New England Biolabs, Ipswich, MA) were transformed, and plasmids were extracted using QIAGEN's HiSpeed Plasmid Midi Kit.

RRAS2 Q72L was generated with Agilent's (Santa Clara, CA) QuikChange Lightning Site Directed Mutagenesis Kit along with RRAS2 forward (5'-tggctccaaactcttctagtcctgctgtatccaaa-3') and reverse (5'-tttggatacagcaggactagaagagtttggagcca-3') primers. The following PCR thermocycler conditions were utilized: initial denaturation (95°C, 2 min), followed by 18 cycles of denaturation (95°C, 20s), annealing (60°C, 10 s) and extension (68°C, 3 min 30s); the reaction was finished after the final extension step (68°C, 5 min). XL10 Gold Ultracompetent cells (Agilent, Santa Clara, CA) were transformed, and plasmids extracted using QIAGEN's HiSpeed Midiprep Kit (Germantown, MD).

Animal Studies

Mice were monitored daily and cared for following guidelines approved by the Memorial Sloan Kettering Institutional Animal Care and Use Committee and Research Animal Resource Center (protocol 04-03-009). Five million Ba/F3 or ten million HBEC cells mixed with 50% (vol/vol) matrigel were implanted via subcutaneous injection into the flank of 6-week-old female NOD-*scid* gamma (NSG) mice (RRID:IMSR_JAX:005557). To test if cell lines formed xenograft tumors cells were injected into two flanks of three mice per cell line (for a total of 6 tumors). For drug treatment studies, mice (five per group) were randomized by tumor size once tumor volume reached 100-150 mm^3. Treatments included once daily (QD) doses via oral gavage of vehicle, 10 mg/kg RMC-6236, 25 mg/kg RMC-6236, or 50 mg/kg RMC-6236. RMC-6236 was reconstituted in 5% DMSO+40%PEG300+5%Tween80+50%ddH_2O. Body weight and tumor size were determined two times per week, with tumor volume calculated with the formula: [length × (width)^2]/2. Animals were monitored daily.

Cell Viability Assays

Cells were plated in 96-well clear bottom, white polystyrene plates at densities of 3,000 (Ba/F3) or 6,000 (HBEC) cells per well and treated with drugs for 96 h. Quantification of viable cells was determined using alamarBlue viability dye (ThermoFisher, Waltham, MA) with fluorescence measured using a Molecular Devices SpectraMax M2 multimodal plate reader (Ex: 555 nm, Em: 585 nm). Data were analyzed with GraphPad Prism

(RRID:SCR_002798) version 10 software by nonlinear regression. Curves were fitted to determine the concentration that inhibits 50% of cell viability (IC_{50}). Data are expressed relative to control values with an average of two to four independent experiments in which each condition was assayed in triplicates.

Western Blotting

For dose-response studies in HBEC cells, 500,000 cell were plated in 6-well dishes and 24 h later cells were deprived of serum for 24 h prior to treatment with inhibitors for 90 min. Cells were washed twice with ice-cold PBS and then lysed with 500 µL 2X LSB buffer supplemented with 7.5% beta mercaptoethanol. Lysates were then passed through an insulin syringe to shear the DNA then heated to 55°C for 15 min. 10-20 µL of lysates were resolved by SDS-PAGE. For dose-response studies in Ba/F3 cells, two million cells were plated in 6-well plates and then deprived of serum for 3 h. Cells were then treated with inhibitors for 90 min, collected by centrifugation and washed twice with ice-cold PBS. Cells were lysed in radioimmunoprecipitation assay (RIPA) buffer supplemented with phosphatase and protease inhibitors (Selleckchem, Houston, TX), and 1 mM sodium orthovanadate (MilliporeSigma, Burlington, MA). For time course studies HBEC cells were serum-starved for 24 h, then treated with 10 nM RMC-6236 for the indicated time periods. Inhibitor was added so that all treatments ended at the same time. Serum-free media with fresh inhibitor was added at each time point. Protein concentration was measured via Bradford assay (Bio-Rad, Hercules, CA). Twenty µg whole-cell lysates per sample were denatured with 2× Laemmli sample buffer for 10 minutes at 55°C and resolved by SDS-PAGE using 4%-12% Bolt gels (ThermoFisher, Waltham, MA). Separated proteins were next transferred onto polyvinylidene fluoride membranes and blocked in 3% (wt/vol) bovine serum albumin (Sigma, Marlborough, MA) solution for 1 h at room temperature before addition of primary antibodies. Membranes were allowed to incubate overnight in primary antibody solution on a shaker at 4°C and then washed three times with Tris-buffered saline supplemented with 0.1% (vol/vol) Tween-20 (Santa Cruz Biotehnology, Santa Cruz, CA). Bound primary antibodies were detected with peroxidase-labeled goat antibody raised against rabbit or mouse IgG (R&D Systems, Minneapolis, MN). Enhanced chemiluminescence Western blotting detection reagent (Cytiva, Marlborough, MA) was added to the samples before capture on radiograph films. Western blot experiments were repeated two times with independently prepared protein samples.

Statistical analysis:

For in vitro IC_{50} determination, normalized values were plotted using a nonlinear regression fit to the normalized data with a variable slope. IC_{50} values were calculated by interpolating the concentration of the compound at which 50% inhibition occurred. 95% confidence intervals (CI) were used to compare efficacy. In animal models, area under curve analysis of tumor volume over time was used to compare treatment responses. All tests of significance were two-tailed, and $P < 0.05$ was considered statistically significant. Error bars represent means $\pm$ standard error of mean (SEM).

RESULTS

RRAS and RRAS2 mutations in NSCLC

From September 2016 to March 2024, 8,488 patients with NSCLC were genomically profiled using MSK-IMPACT with full coverage of *RRAS* and *RRAS2* exons. In total, mutations in *RRAS* and *RRAS2* were detected in 40 and 41 patients, respectively. In *RRAS*, there was clear predominance of a hotspot missense mutation (c.260A>T, p.Q87L) that was present in 16 samples **(Figure 1A, top panel)**. All other mutations were observed only once. The RRAS Q87 residue is analogous to Q61 in classical RAS proteins, while RRAS G38 and G39 correspond to RAS G12 and G13, respectively **(Figure 1B)**. One case showed *RRAS* p.G38D, and another showed p.G39V. In *RRAS2*, there was an equally notable hotspot mutation (c.215A>T, p.Q72L) observed in 22 samples **(Figure 1A, bottom panel)**. *RRAS2* p.Q72H was seen in one sample. As in *RRAS*, this hotspot mutation occurred in a residue analogous to Q61 in classical RAS proteins **(Figure 1B)**. In contrast to Q72, analysis of G23 and G24 residues in RRAS2 (corresponding to G12 and G13 in classical RAS, respectively) showed only rare substitutions at low frequencies (p.G23C, n=1; p.G23V, n=1; p.G24C, n=2; p.G24V, n=1) similar to the background rates for variants of unknown significance. Taken together, the two dominant hotspot mutations, *RRAS*^{Q87L} and *RRAS2*^{Q72L}, were detected in 0.45% of patients with NSCLC (38/8,488). Given the strikingly recurrent nature of *RRAS*^{Q87L} and *RRAS2*^{Q72L} mutations, patient samples with these variants were further analyzed as separate cohorts.

Clinical, pathologic, and genomic characteristics of *RRAS*^{Q87L} and *RRAS2*^{Q72L}-mutated NSCLC. The median age at diagnosis for patients with *RRAS*^{Q87L}-mutated lung cancers was 77.5 years, while those with *RRAS2*^{Q72L}-mutated tumors was 70.5 years **(Table 1)**. The majority of patients with either mutation was female with a positive smoking history. Most patients had early-stage tumors. Indeed, two *RRAS*^{Q87L} mutations were found in lung adenocarcinoma in situ (AIS). A review of tumor histology revealed that nearly all cases were comprised of lung adenocarcinomas (LUADs) (15/16, *RRAS*^{Q87L} and 19/22, *RRAS2*^{Q72L}) **(Figure 1C-D)**. The other patients had pleomorphic carcinoma of the lung (n=1, *RRAS*^{Q87L} and n=1, *RRAS2*^{Q72L}) and lung squamous cell carcinoma (n=2, *RRAS2*^{Q72L}).

Focusing on LUAD, the most common histologic subtype, the combined frequency of *RRAS*^{Q87L} and *RRAS2*^{Q72L} mutations was 0.53% in LUAD patients screened for *RRAS* and *RRAS2* mutations (34/6,359). Among resected invasive LUADs, IASLC grade 3 was seen in 50% of *RRAS*^{Q87L}-mutated cases and 36% of *RRAS2*^{Q72L}-mutated cases. The majority of tumors were negative for PD-L1 expression by immunohistochemistry (71% and 59% PD-L1 negative among *RRAS*^{Q87L} and *RRAS2*^{Q72L} cases, respectively) and median tumor mutational burdens (TMB) for *RRAS*^{Q87L} and *RRAS2*^{Q72L} were 7.2 and 5.1 muts/Mb, respectively. Remarkably, all tumors with *RRAS*^{Q87L} lacked other canonical activating alterations in the receptor tyrosine kinase (RTK)/RAS/RAF pathway. Similarly, tumors with *RRAS2*^{Q72L} were also wild type for other activating RTK/RAS/RAF alterations, with the exception of two cases that had concurrent MAPK pathway mutations: one KRAS^{G12V} and one MET exon 14 skipping mutation. Other recurrently co-altered genes included *TP53*, *RBM10*, *CDKN2A*, *TERT* and *ATM* **(Figure 1E)**.

To assess the clinico-genomic features associated with *RRAS*^{Q87L} and *RRAS2*^{Q72L} mutations, we compared our cohorts with a stage-matched control group of LUADs lacking *RRAS*^{Q87L} and *RRAS2*^{Q72L} mutations. The clinical and molecular characteristics of this cohort have been published previously.[34] Comparative analysis revealed that patients with *RRAS*^{Q87L} and *RRAS2*^{Q72L} were older than patients with no mutations in these two genes. In addition, patients with *RRAS2*^{Q72L} mutations were more likely to be women compared to the control group. There

were no other significant differences in clinical, pathologic, and genomic features, including co-mutational landscapes. The full demographic, clinical and genomic characteristics of patients with *RRAS*^{Q87L} and *RRAS2*^{Q72L} are provided in **Supplemental Table 3A**.

RRAS and *RRAS2* mutations in other large WES cohorts

To further explore the characteristics of *RRAS* and *RRAS2* mutations and to correlate our findings with those from other independent cohorts, we searched for *RRAS* and *RRAS2* mutations in the TCGA WES LUAD (n=566) and LUSC (n=484) series. In total, three *RRAS* and five *RRAS2* mutations were identified. *RRAS*^{Q87L} and *RRAS2*^{Q72L} were the most common and only recurrent mutations, with each variant seen in two cases. The other remaining mutations were observed once and were all classified as variants of unknown significance. Notably, mutations involving p.G38/G39 in *RRAS* and p.G23/G24 in *RRAS2* (corresponding to p.G12/G13 in classical RAS) were not seen in those lung cancer cohorts. In terms of histology, both mutations were present equally in LUAD and LUSC. Similar to the MSK cases, all tumors with *RRAS*^{Q87L} and *RRAS2*^{Q72L} lacked other activating alterations in the RTK/RAS/RAF pathway. In addition to the TCGA cohorts, we searched for *RRAS* and *RRAS2* mutations in another large WES LUAD series (OncoSG, n=302). In this series, *RRAS2*^{Q72L} was identified in a single tumor that was also wild type for activating alterations in other RTK/RAS/RAF genes. Taken together, the overall frequency of *RRAS*^{Q87L} and *RRAS2*^{Q72L} was 0.37% within NSCLC cases (5/1,352) and 0.35% within LUAD (3/868), from the respective WES cohorts. This was largely concordant with the frequencies observed in the MSK series. The full clinical and pathologic features of *RRAS*^{Q87L}- and *RRAS2*^{Q72L}-mutated NSCLC cases from other WES cohorts are provided in **Supplemental Table 3B**.

RRAS^{Q87L} and RRAS2^{Q72L} are oncogenic and targetable mutations in Ba/F3 cells

To investigate the oncogenic potential of these clinically identified *RRAS* and *RRAS2* mutations *in vitro*, we first expressed the mutations of interest in the murine pro-B cell line Ba/F3 and HEK-293T cells. Ba/F3 cells are a popular model for studying oncogenesis due to their dependence on interleukin-3 (IL-3) for proliferation and loss of this dependency when cells are transformed with oncogenes.[35] Expression of RRAS^{Q87L} or RRAS2^{Q72L} in Ba/F3 cells resulted in IL-3-independent growth while growth of cells expressing an empty vector or wild-type RRAS or RRAS2 was halted when IL-3 was depleted (**Figure 2A**). Ba/F3 cells expressing RRAS^{Q87L} or RRAS2^{Q72L} formed tumors in NSG mice (**Supplemental Figure 1**). Increased phosphorylation of ERK1/2, AKT, and the downstream effectors S6 and p90 RSK was observed in HEK-293T and Ba/F3 cells expressing RRAS^{Q87L} or RRAS2^{Q72L} compared to cells expressing the wildtype counterparts (**Supplemental Figure 1, Figure 2B**).

We next sought to identify therapeutic vulnerabilities of Ba/F3 cells expressing RRAS^{Q87L} or RRAS2^{Q72L} utilizing MAPK-targeted therapies including RMC-6236. RMC-6236 is a first-in-class, multi-selective inhibitor of GTP-bound RAS targeting the active state of multiple members of the RAS family, including both wild-type and mutant variants.[10,36] The preclinical efficacy of RMC-6236 has been demonstrated in cells harboring mutant KRAS, NRAS, and HRAS with mutations at codon positions G12, G13, and Q61. We thus set out to determine if RMC-6236 also possesses activity against RRAS and RRAS2 mutants to potentially expand the use of this class of inhibitors to additional members of the RAS superfamily. RMC-6236 is currently under investigation in multiple clinical trials (NCT05379985, NCT06625320, NCT06040541; NCT06162221; NCT06445062; NCT06128551).

Western blotting analysis of cell extracts prepared from Ba/F3 cells expressing either wild-type or mutant RRAS/RRAS2 indicated that RRAS- and RRAS2-mutant cells treated with RMC-6236 exhibited diminished phosphorylation of ERK1/2, AKT and S6 in a dose-dependent manner (**Figure 2C**). The capacity of RMC-6236 to inhibit activation of members of both the MAPK and PI3K-AKT pathway has also been demonstrated in cell models of $KRAS^{G12X}$.[36] RMC-6236 was more effective at blocking ERK1/2 phosphorylation in $RRAS2^{Q72L}$- expressing Ba/F3 cells (**Figure 2C**) relative to those expressing wild-type RRAS2 (Supplemental Figure 2), whereas $RRAS^{Q87L}$ and RRAS wild-type-expressing cells underwent a similar degree of ERK1/2 phosphorylation blockade **(Figure 2C and Supplemental Figure 2)**. In concordance with this data, $RRAS^{Q87L}$ and $RRAS2^{Q72L}$ mutants demonstrated enhanced sensitivity to targeted inhibitors of MEK1/2 (binimetinib), ERK1/2 (SHC772984, ulixertinib), and RAS (RMC-6236) relative to Ba/F3 cells with overexpression of wild-type RRAS and RRAS2 (**Figure 2D and Supplemental Table 4**).

Human lung cells expressing $RRAS^{Q87L}$ or $RRAS2^{Q72L}$ are transformed and sensitive to RMC-6236

We next set out to investigate the effect of overexpression of $RRAS^{Q87L}$ or $RRAS2^{Q72L}$ in an immortalized non-transformed human lung cancer cell line [(human bronchiolar epithelial cells (HBEC)]. $RRAS^{Q87L}$ and $RRAS2^{Q72L}$ were again sufficient to transform HBEC cells *in vivo*, with tumor formation following subcutaneous injection into NSG mice **(Figure 3A)**. HBEC-$RRAS2^{Q72L}$ xenograft tumors grew faster than HBEC-$RRAS^{Q87L}$. Similar to Ba/F3 cells, HBEC cells overexpressing the *RRAS* and *RRAS2* mutants had enhanced activation of ERK1/2 and downstream signaling proteins such as S6 and p90 RSK, as well as activation of AKT, P70, and STAT3 **(Figure 3B)**. HBEC cells expressing mutant RRAS/RRAS2 showed upregulation of negative regulators of the MAPK pathway, including SPRED1, SPRY1, and SPRY2 **(Figure 3B)**. Increased expression of DUSP6 was more prominent in cells expressing $RRAS2^{Q72L}$ compared to cells expressing wild-type RRAS/RRAS2 or $RRAS^{Q87L}$ **(Figure 3B)**. It is possible that the negative regulators of the MAPK pathway were upregulated to restrain activation of MEK1/2 and ERK1/2, thereby preventing cell death or senescence due to ERK hyperactivation. This phenomenon has been observed in other models of RAS-driven cancer, including pancreatic and colorectal cancers.[37,38]

$RRAS^{Q87L}$ and $RRAS2^{Q72L}$ mutant HBECs treated with RMC-6236 demonstrated diminished phosphorylation of ERK1/2 and P90 in a dose-dependent fashion, though phosphorylation of AKT and the downstream regulator S6 showed no reduction **(Figure 3C)**. Treatment with 10 nM RMC-6236 over a 48-hour time course also resulted in sustained inhibition of ERK1/2 and p90 RSK phosphorylation, downregulation of negative regulators of the MAPK pathway and markers of cell cycle progression, and upregulation of pro-apoptotic proteins **(Figure 3D).** HBEC cells harboring $RRAS^{Q87L}$ or $RRAS^{Q87L}$ exhibited enhanced sensitivity to inhibitors of the MAPK pathway relative to cells expressing the wild-type counterparts **(Figure 3E and Supplemental Table 4)**.

To investigate *in vivo* efficacy of RMC-6236, NSG mice bearing HBEC-$RRAS^{Q87L}$ or HBEC-$RRAS2^{Q72L}$ xenograft tumors were treated with vehicle or 10 mg/kg-50 mg/kg RMC-6236 once daily. Tumor volume over time is shown in **Figure 4A** and area under cure analysis of the tumor growth data is shown in **Figure 4B**. In both xenograft models RMC-6236 caused a significant reduction in tumor growth compared to vehicle-treated animals. However, the dose of 25 mg/kg

was as effective as 50 mg/kg **(Figure 4A-C)**. No reduction in animal weight **(Supplemental Figure 3)** or dose-dependent toxicity was observed up to 50 mg/kg.

DISCUSSION

Our data nominates RRAS^{Q87L} and RRAS2^{Q72L} as novel and recurrent oncogenic drivers in lung cancers, present in approximately 0.37-0.45% of NSCLC samples in the MSK-IMPACT cohort and other large WES NSCLC series. The observed prevalence of RRAS^{Q87L} and RRAS2^{Q72L} is similar to other well-studied but uncommon driver oncogenes in NSCLC including HRAS, NRAS, ROS1, NTRK, and NRG1, all present at approximately 0.1-1% frequency.[39] Importantly, RRAS^{Q87L} or RRAS2^{Q72L} mutations were largely exclusive with other activating RTK-RAS-RAF alterations, suggesting that these mutations represent the primary oncogenic driver. A smaller number of identified RRAS/RRAS2 mutations homologous to other KRAS hotspots (RRAS$^{G38/G39}$ and RRAS2$^{G23/G24}$) were also identified in this study but these mutations were not highly recurrent. It remains uncertain if these latter mutations play a cooperative role in tumorigenesis.

Expression of RRAS^{Q87L} or RRAS2^{Q72L} alone were sufficient to transform murine Ba/F3 cells and human lung cells. RRAS2^{Q72L} has previously been identified as capable of forming tumors *in vivo*,[40] though our study is the first direct demonstration of the oncogenic role of RRAS^{Q87L}. These mutations resulted in activation of both the MAPK and AKT/PI3K signaling axes, as well as potently upregulating negative regulators of MAPK function. Upregulation of these MAPK negative regulators may be necessary to prevent hyperactivation of ERK1/2, which can be toxic to cells. Our data suggest mutated RRAS/RRAS2 are capable of driving oncogenicity in a manner similar to other RAS-family members.[41] Importantly, RRAS^{Q87L} and RRAS2^{Q72L} mutants were sensitive to targeted inhibitors of the MAPK pathway, including inhibition of RAS (RMC-6236), MEK1/2 (binimetinib), and ERK1/2 (SCH772984 and ulixertinib). Of these therapies, binimetinib, in combination with encorafenib, is currently FDA-approved for use in the treatment of BRAF^{V600E}-mutant NSCLC and could potentially be used off-label for patients with RRAS/RRAS2-driven lung cancer. Though targeted therapies against members of the MAPK pathway often show excellent preclinical efficacy in RAS-driven models of lung cancers, the clinical efficacy of these inhibitors is often hampered by various drug resistance mechanisms including on-target mutations or re-wiring of growth factor signaling.[42-44] In an effort to overcome common drug resistance mechanisms as well as target multiple RAS isoforms, RMC-6236 was developed as a first-in-class, non-covalent inhibitor of GTP-bound RAS. RMC-6236 has shown efficacy in preclinical models with K/H/N-RAS, including settings of resistance to other RAS inhibitors.[36] RMC-6236 is currently under investigation in multiple clinical trials of RAS mutant solid tumors including NSCLC, pancreatic, and GI cancers. Available analysis from an ongoing phase 1/1b clinical trial (NCT05379985) shows promising efficacy in previously treated, RAS-mutant pancreatic adenocarcinoma patients, with median progression-free survival of 8.5 months and 7.6 months in KRAS G12X and RAS mutant, respectively.[45] A randomized phase 3 trial is currently underway to evaluate RMC-6236 versus standard chemotherapy in pre-treated patients with metastatic pancreatic adenocarcinoma (NCT06625320).

In RRAS^{Q87L} and RRAS2^{Q72L}-mutant HBEC cell lines, phosphorylation of ERK1/2 and its downstream effector p90 RSK was potently inhibited by RMC-6236 at similar concentrations required in KRAS^{G12}-mutant models. In HBEC-RRAS^{Q87L} and HBEC-RRAS2^{Q72L} xenograft tumors, RMC-6236 inhibited tumor growth in a dose-dependent fashion (10 mg/kg – 50 mg/kg). Although dose titration to maximize clinical efficacy with a favorable tolerability profile is still ongoing, current trials of RMC-6236 monotherapy are utilizing daily dosing between 120-300 mg. Previous pharmacokinetic modeling has estimated the 300 mg daily dosing in humans would be needed to reach an equivalent mean blood exposure observed in mice treated with the 25 mg/kg daily dosing schedule.[36] Hence, RMC-6236 appears to be active in RRAS and RRAS2-mutant cells at clinically achievable concentrations, though whether differences in activity compared to KRAS-mutant models is clinically significant remains to be determined.

Nevertheless, the similar signaling profiles and drug sensitivities observed in RRAS and RRAS2 mutant models relative to KRAS warrant inclusion of these mutations in the broader study of RAS-driven cancers.

The introduction of targeted therapies as front-line management of oncogene-positive advanced NSCLCs has revolutionized lung cancer treatment in the past two decades. However, there still remains approximately 20-30% of NSCLC tumors that lack a routinely identified actionable oncogenic driver.[39] There exists a pressing need to continue identifying actionable driver alterations in order for these patients to reap the benefits of existing and novel targeted therapies. By leveraging a comprehensive NGS panel that is designed for both clinical actionability and biomarker discovery, we have identified, for the first time, $RRAS^{Q87L}$ and $RRAS2^{Q72L}$ as recurrent mutations in driver-negative NSCLCs at frequencies that are similar to NTRK and NRG1 fusions. Importantly, our experimental and functional data show these mutations as oncogenic drivers that are sensitive to the novel and clinically-active pan-RAS inhibitor RMC-6236. Taken together, our findings delineate a novel cohort of patients with $RRAS^{Q87L}$- and $RRAS2^{Q72L}$-mutant lung cancers who may be potential candidates for future trials of RAS-targeted therapies. Notably, given that *RRAS* and *RRAS2* are not profiled on most NGS panels, addition of these genes in clinical sequencing panels should be considered in order to expand screening and to advance treatment strategies for patients with $RRAS^{Q87L}$ and $RRAS2^{Q72L}$-mutated lung cancers.

ACKNOWLEDGEMENTS

This research was partly supported by a grant from the Department of Pathology and Laboratory Medicine at MSK (to SRY) and grants from the National Cancer Institute of the National Institutes of Health, P30 CA008748 (Cancer Center Support grant to MSK), 5R25CA020449 (Medical summer student research support for AJP, TZ, RC, RPM), and 5P01CA129243-13 (ML). The authors thank Tracey Riano for administrative help with the Medical Summer Student Research Program.

Conflict of interest disclosure

Alexander J. Pfeil, Tom Zhang, Ryan Cheng, Marissa S. Mattar, Leo Gili, Rachel Lai, Inna Khodos, Rohan P. Master, Jenna-Marie Dix, Andrea Gazzo, Kathryn C. Arbour, Elisa de Stanchina and Christopher A. Febres-Aldana report no potential conflict of interest.

Soo-Ryum Yang reports honoraria from Medscape, Medical Learning Institute, PRIME Education, and consulting for AstraZeneca, AbbVie, Merus, Roche, Amgen, and Sanofi.

Marc Ladanyi received advisory board compensation from Boehringer Ingelheim, AstraZeneca, Bristol-Myers Squibb, Takeda, and Bayer, and research support from LOXO Oncology and Helsinn Healthcare.

Romel Somwar received research grants from Helsinn Healthcare, SA, LOXO Oncology, Elevation Oncology, and Merus, all unrelated to the current study.

REFERENCES

1. Ma F, Laster K, Dong Z. The comparison of cancer gene mutation frequencies in Chinese and US patient populations. *Nature Communications*. 2022;13(1):5651.
2. Prior IA, Hood FE, Hartley JL. The frequency of Ras mutations in cancer. *Cancer research*. 2020;80(14):2969-2974.
3. Jeon H, Tkacik E, Eck MJ. Signaling from RAS to RAF: the molecules and their mechanisms. *Annual Review of Biochemistry*. 2024;93
4. Takács T, Kudlik G, Kurilla A, Szeder B, Buday L, Vas V. The effects of mutant Ras proteins on the cell signalome. *Cancer and Metastasis Reviews*. 2020;39:1051-1065.
5. Colicelli J. Human RAS superfamily proteins and related GTPases. *Science's STKE*. 2004;2004(250):re13-re13.
6. Timar J, Kashofer K. Molecular epidemiology and diagnostics of KRAS mutations in human cancer. *Cancer and Metastasis Reviews*. 2020;39(4):1029-1038.
7. Prior IA, Lewis PD, Mattos C. A comprehensive survey of Ras mutations in cancer. *Cancer research*. 2012;72(10):2457-2467.
8. Kwan AK, Piazza GA, Keeton AB, Leite CA. The path to the clinic: a comprehensive review on direct KRASG12C inhibitors. *Journal of Experimental & Clinical Cancer Research*. 2022;41(1):27.
9. Lim TKH, Skoulidis F, Kerr KM, Ahn M-J, Kapp JR, Soares FA, Yatabe Y. KRAS G12C in advanced NSCLC: prevalence, co-mutations, and testing. *Lung Cancer*. 2023;184:107293.
10. Holderfield M, Lee BJ, Jiang J, et al. Concurrent inhibition of oncogenic and wild-type RAS-GTP for cancer therapy. *Nature*. 2024:1-8.
11. Weber SM, Carroll SL. The role of R-Ras proteins in normal and pathologic migration and morphologic change. *The American Journal of Pathology*. 2021;191(9):1499-1510.
12. Self AJ, Caron E, Paterson HF, Hall A. Analysis of R-Ras signalling pathways. *Journal of Cell Science*. 2001;114(7):1357-1366.
13. Marte BM, Rodriguez-Viciana P, Wennström S, Warne PH, Downward J. R-Ras can activate the phosphoinositide 3-kinase but not the MAP kinase arm of the Ras effector pathways. *Current Biology*. 1997;7(1):63-71.
14. Huff SY, Quilliam LA, Cox AD, Der CJ. R-Ras is regulated by activators and effectors distinct from those that control Ras function. *Oncogene*. 1997;14(2):133-143.
15. Keely PJ, Rusyn EV, Cox AD, Parise LV. R-Ras signals through specific integrin α cytoplasmic domains to promote migration and invasion of breast epithelial cells. *The Journal of cell biology*. 1999;145(5):1077-1088.
16. Movilla N, Crespo P, Bustelo XR. Signal transduction elements of TC21, an oncogenic member of the R-Ras subfamily of GTP-binding proteins. *Oncogene*. 1999;18(43):5860-5869.
17. Rodriguez-Viciana P, Sabatier C, McCormick F. Signaling specificity by Ras family GTPases is determined by the full spectrum of effectors they regulate. *Molecular and cellular biology*. 2004;
18. Graham SM, Vojtek AB, Huff SY, Cox AD, Clark GJ, Cooper JA, Der CJ. TC21 causes transformation by Raf-independent signaling pathways. *Molecular and cellular biology*. 1996;16(11):6132-6140.

19. Cox A, Brtva T, Lowe D, Der C. R-Ras induces malignant, but not morphologic, transformation of NIH3T3 cells. *Oncogene*. 1994;9(11):3281-3288.
20. Graham SM, Cox AD, Drivas G, Rush MG, D'Eustachio P, Der CJ. Aberrant function of the Ras-related protein TC21/R-Ras2 triggers malignant transformation. *Molecular and cellular biology*. 1994;
21. Saez R, Chan A, Miki T, Aaronson SA. Oncogenic activation of human R-ras by point mutations analogous to those of prototype H-ras oncogenes. *Oncogene*. 1994;9(10):2977-2982.
22. Cifuentes C, Oeste CL, Fernández-Pisonero I, et al. Unmutated RRAS2 emerges as a key oncogene in post-partum-associated triple negative breast cancer. *Molecular Cancer*. 2024;23(1):142.
23. Hortal AM, Oeste CL, Cifuentes C, et al. Overexpression of wild type RRAS2, without oncogenic mutations, drives chronic lymphocytic leukemia. *Molecular cancer*. 2022;21(1):35.
24. Clark GJ, Kinch MS, Gilmer TM, Burridge K, Der CJ. Overexpression of the Ras-related TC21/R-Ras2 protein may contribute to the development of human breast cancers. *Oncogene*. 1996;12(1):169-176.
25. Schulte SL, Waha A, Steiger B, et al. CNS germinomas are characterized by global demethylation, chromosomal instability and mutational activation of the Kit-, Ras/Raf/Erk-and Akt-pathways. *Oncotarget*. 2016;7(34):55026.
26. Mata DA, Yang S-R, Ferguson DC, et al. RAS/MAPK pathway driver alterations are significantly associated with oncogenic KIT mutations in germ-cell tumors. *Urology*. 2020;144:111-116.
27. Flex E, Jaiswal M, Pantaleoni F, et al. Activating mutations in RRAS underlie a phenotype within the RASopathy spectrum and contribute to leukaemogenesis. *Human molecular genetics*. 2014;23(16):4315-4327.
28. Capri Y, Flex E, Krumbach OH, et al. Activating mutations of RRAS2 are a rare cause of Noonan syndrome. *The American Journal of Human Genetics*. 2019;104(6):1223-1232.
29. Cheng DT, Mitchell TN, Zehir A, et al. Memorial Sloan Kettering-Integrated Mutation Profiling of Actionable Cancer Targets (MSK-IMPACT): a hybridization capture-based next-generation sequencing clinical assay for solid tumor molecular oncology. *The Journal of molecular diagnostics*. 2015;17(3):251-264.
30. Chakravarty D, Gao J, Phillips S, et al. OncoKB: a precision oncology knowledge base. *JCO precision oncology*. 2017;1:1-16.
31. Chang MT, Bhattarai TS, Schram AM, et al. Accelerating discovery of functional mutant alleles in cancer. *Cancer discovery*. 2018;8(2):174-183.
32. WHO Classification of Tumours Editorial Board. Thoracic Tumours. 5th ed. Lyon, France: International Agency for Research on Cancer; 2021
33. Moreira AL, Ocampo PS, Xia Y, et al. A grading system for invasive pulmonary adenocarcinoma: a proposal from the International Association for the Study of Lung Cancer Pathology Committee. *Journal of Thoracic Oncology*. 2020;15(10):1599-1610.
34. Lengel HB, Mastrogiacomo B, Connolly JG, et al. Genomic mapping of metastatic organotropism in lung adenocarcinoma. *Cancer Cell*. 2023;41(5):970-985. e3.

35. Koga T, Suda K, Mitsudomi T. Utility of the Ba/F3 cell system for exploring on‐target mechanisms of resistance to targeted therapies for lung cancer. *Cancer Science*. 2022;113(3):815-827.
36. Jiang J, Jiang L, Maldonato BJ, et al. Translational and therapeutic evaluation of RAS-GTP inhibition by RMC-6236 in RAS-driven cancers. *Cancer Discovery*. 2024;14(6):994-1017.
37. Yip-Schneider MT, Lin A, Marshall MS. Pancreatic tumor cells with mutant K-ras suppress ERK activity by MEK-dependent induction of MAP kinase phosphatase-2. *Biochemical and biophysical research communications*. 2001;280(4):992-997.
38. Cagnol S, Rivard N. Oncogenic KRAS and BRAF activation of the MEK/ERK signaling pathway promotes expression of dual-specificity phosphatase 4 (DUSP4/MKP2) resulting in nuclear ERK1/2 inhibition. *Oncogene*. 2013;32(5):564-576.
39. Chevallier M, Borgeaud M, Addeo A, Friedlaender A. Oncogenic driver mutations in non-small cell lung cancer: Past, present and future. *World Journal of Clinical Oncology*. 2021;12(4):217.
40. Fernandez-Pisonero I, Clavaín L, Robles-Valero J, et al. A hotspot mutation targeting the R-RAS2 GTPase acts as a potent oncogenic driver in a wide spectrum of tumors. *Cell Reports*. 2022;38(11)
41. Kim HJ, Lee HN, Jeong MS, Jang SB. Oncogenic KRAS: signaling and drug resistance. *Cancers*. 2021;13(22):5599.
42. Tsao M-S, Sakurada A, Cutz J-C, et al. Erlotinib in lung cancer—molecular and clinical predictors of outcome. *New England Journal of Medicine*. 2005;353(2):133-144.
43. Arcila ME, Oxnard GR, Nafa K, et al. Rebiopsy of lung cancer patients with acquired resistance to EGFR inhibitors and enhanced detection of the T790M mutation using a locked nucleic acid-based assay. *Clinical cancer research*. 2011;17(5):1169-1180.
44. Kulkarni A, Al-Hraishawi H, Simhadri S, et al. BRAF fusion as a novel mechanism of acquired resistance to vemurafenib in BRAF V600E mutant melanoma. *Clinical Cancer Research*. 2017;23(18):5631-5638.
45. Garrido-Laguna I, Wolpin BM, Park W, et al. Safety, efficacy, and on-treatment circulating tumor DNA (ctDNA) changes from a phase 1 study of RMC-6236, a RAS (ON) multi-selective, tri-complex inhibitor, in patients with RAS mutant pancreatic ductal adenocarcinoma (PDAC). American Society of Clinical Oncology; 2025.

TABLES

Characteristics	**RRAS p.Q87L NSCLC (n=16)**		**RRAS2 p.Q72L NSCLC (n=22)**		**RRAS/RRAS2 wild type LUAD (n=520)**
Clinical data		P value		P value	
Median age, years (range)	77.5 (54-86)	0.00002	70.5 (61-81)	0.04	67.2 (27.5-92.2)
Sex					
Female	10 (63%)	1	19 (86%)	0.04	336 (65%)
Male	6 (38%)		3 (14%)		184 (35%)
Smoking					
Ever	15 (94%)	0.05	19 (86%)	0.2	318 (71%)
Never	1 (6%)		3 (14%)		127 (29%)
Clinical stage					
AIS	2 (13%)	0.2	0 (0%)	0.2	0 (0%)
I	9 (56%)		10 (45%)		275 (53%)
II	0 (0%)		2 (9%)		61 (12%)
III	3 (19%)		6 (27%)		58 (11%)
IV	2 (13%)		4 (18%)		126 (24%)
Pathologic data		-		-	
Histology					
LUAD	15 (94%)		19 (86%)		520 (100%)
LUSC	0 (0%)		2 (9%)		0 (0%)
Pleomorphic	1 (6%)		1 (5%)		0 (0%)
IASLC grade*		-		-	
1	0 (0%)		4 (36%)		NA
2	3 (50%)		3 (27%)		NA
3	3 (50%)		4 (36%)		NA
Biomarker data					
PD-L1 IHC					
Positive	4 (29%)	-	9 (41%)	-	NA
Negative	10 (71%)		13 (59%)		NA
Median TMB, muts/Mb (range)	7.2 (0.8-26.3)	0.09	5.1 (0.9-29.7)	0.9	5.2 (0-59.7)

Table 1: *IASLC grades were assessed for resected invasive LUADs. PD-L1 positivity was defined as having a score of ≥1%. AIS and stage I have been combined for comparison of clinical stage. Abbreviations: AIS=adenocarcinoma in situ; LUAD=lung adenocarcinoma; LUSC=lung squamous cell carcinoma; IHC=immunohistochemistry; TMB=tumor mutational burden.

FIGURE LEGENDS

Figure 1. Characterization of *RRAS* and *RRAS2* mutations in lung cancer
A). Lollipop figure of *RRAS* mutations in NSCLC, demonstrating a clear hotspot in RRAS p.Q87L (top panel) and a lollipop figure of *RRAS2* mutations in NSCLC, with a similarly striking hotspot mutations in *RRAS2* p.Q72L (bottom panel). Single case of *RRAS2* p.Q72H not shown. **B**). Primary amino acid sequence alignment of KRAS, NRAS, HRAS, RRAS, and RRAS2. Conservation represents the similarity of residues at each position by height. **C**). Lung adenocarcinoma with micropapillary pattern and an RRAS c.260A>T, p.Q87L mutation. **D**) Lung adenocarcinoma with lepidic pattern and an RRAS2 c.215A>T, p.Q72L mutation. Images captured at 10x. **E**). Oncoprint of NSCLC with *RRAS* p.Q87L (left panel) and *RRAS2* p.Q72L (right panel). TMB measured in muts/Mb. aa=amino acid; RTK=receptor tyrosine kinase; TMB=tumor mutational burden; LUAD=lung adenocarcinoma; PLC=pleomorphic carcinoma of the lung; LUSC=lung squamous cell carcinoma

Figure 2. Expression of RRAS^{Q87L} or RRAS2^{Q72L} is oncogenic in Ba/F3 cells
A). Ba/F3 cells expressing an empty vector (EV), wild-type (WT) RRAS/RRAS2, or mutant RRAS/RRAS2 were grown in media with or without 5 ng/mL IL-3. **B**). Whole-cell extracts from the isogenic Ba/F3 cells were resolved by SDS-PAGE and immunoblotted for the indicated proteins. Representative immunoblots from two independent experiments are shown. **C**). Isogenic Ba/F3 cells were treated for 90 mins with the indicated doses of RMC-6236 and then whole-cell extracts were prepared and subjected to Western blotting. Representative immunoblots from two independent experiments are shown. **D**) The indicated Ba/F3 cell lines were treated for 96 h with inhibitors of ERK1/2 (SHC772984, ulixertinib), MEK1/2 (binimetinib), or RAS (RMC-6236). Results represent the mean ± SEM of three independent experiments where each condition was assayed in triplicates. IC_{50} values for growth inhibition are given in **Supplemental Table 4.**

Figure 3. Human bronchiolar epithelial cells expressing RRAS^{Q87L} or RRAS2^{Q72L} are oncogenic and sensitive to pan-RAS inhibition
A). Tumor growth in NSG mice following subcutaneous injection of HBEC cells expressing an empty vector (EV), RRAS/RRAS2 wild type (WT), or mutant RRAS/RRAS2. Data represent the mean ± SEM of six tumors. **B**). Whole-cell extracts were subjected to Western blot analysis. Representative immunoblots from two independent experiments are shown. **C**). Cells were treated for 90 mins with the indicated concentrations of RMC-6236 and then whole-cell extracts were prepared and subjected to Western blot analysis. Representative immunoblots from two independent experiments are shown **D**). Cells were treated for the indicated times with 10 nM RMC-6236 prior to preparation of whole cells extracts and Western blot analysis. Representative immunoblots from two independent experiments are shown. **E**). Isogenic HBEC cells were treated for 96 h with the indicated concentrations of inhibitors targeting ERK1/2 (SHC772984, ulixertinib), MEK1/2 (binimetinib), or RAS (RMC-6236). Results represent the mean ± SD of 2 independent experiments in which there were three replicates of each condition. IC_{50} values for growth inhibition are given in **Supplemental Table 4**.

Figure 4. RMC-6236 is effective therapy in *in vivo* models of **RRAS^{Q87L} or RRAS2^{Q72L} driven lung cancer**
A). Tumor growth in immunocompromised NSG mice treated with RMC-6236 (vehicle, 10 mg/kg, 25 mg/kg, or 50 mg/kg, once daily). **B**). Area under curve analysis of tumor volume over the treatment course . Results represent the mean ± SEM of five tumors. Tumor volumes compared with one-way ANOVA with Tukey's multiple comparisons test. The vehicle treated group of RRAS2^{Q72L}-tumor bearing mice demonstrated an area under the curve which was

greater than each of the treatment groups with a p-value <0.0001 (p-values not shown) **C**). Fraction of tumor volume change from baseline (expressed as %) of individual tumors. The average ± SEM reduction of the group is shown above the bars. Effect of RMC-6236 on animal weight is shown in **Supplemental Figure 3.**

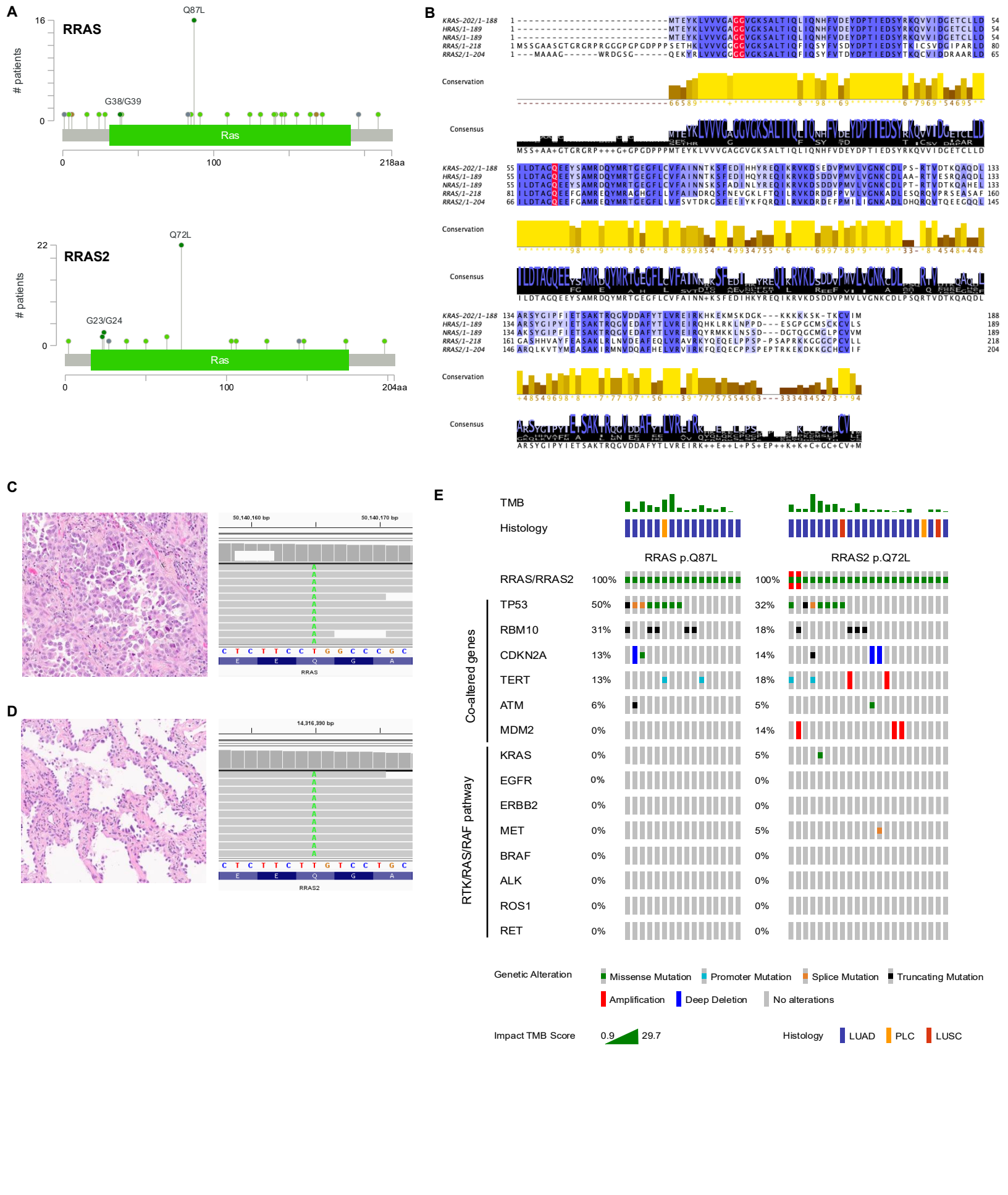
A
RRAS
Q87L
G38/G39
patients
16
0
Ras
0
100
218aa
RRAS2
Q72L
G23/G24
22
0
Ras
0
100
204aa
B
KRAS-202/1-188
HRAS/1-189
NRAS/1-189
RRAS/1-218
RRAS2/1-204
Conservation
Consensus
C
50,140,160 bp
50,140,170 bp
RRAS
D
14,316,390 bp
RRAS2
E
TMB
Histology
RRAS p.Q87L
RRAS2 p.Q72L
RRAS/RRAS2
Co-altered genes
TP53
RBM10
CDKN2A
TERT
ATM
MDM2
RTK/RAS/RAF pathway
KRAS
EGFR
ERBB2
MET
BRAF
ALK
ROS1
RET
Genetic Alteration
Missense Mutation
Promoter Mutation
Splice Mutation
Truncating Mutation
Amplification
Deep Deletion
No alterations
Impact TMB Score
0.9
29.7
Histology
LUAD
PLC
LUSC

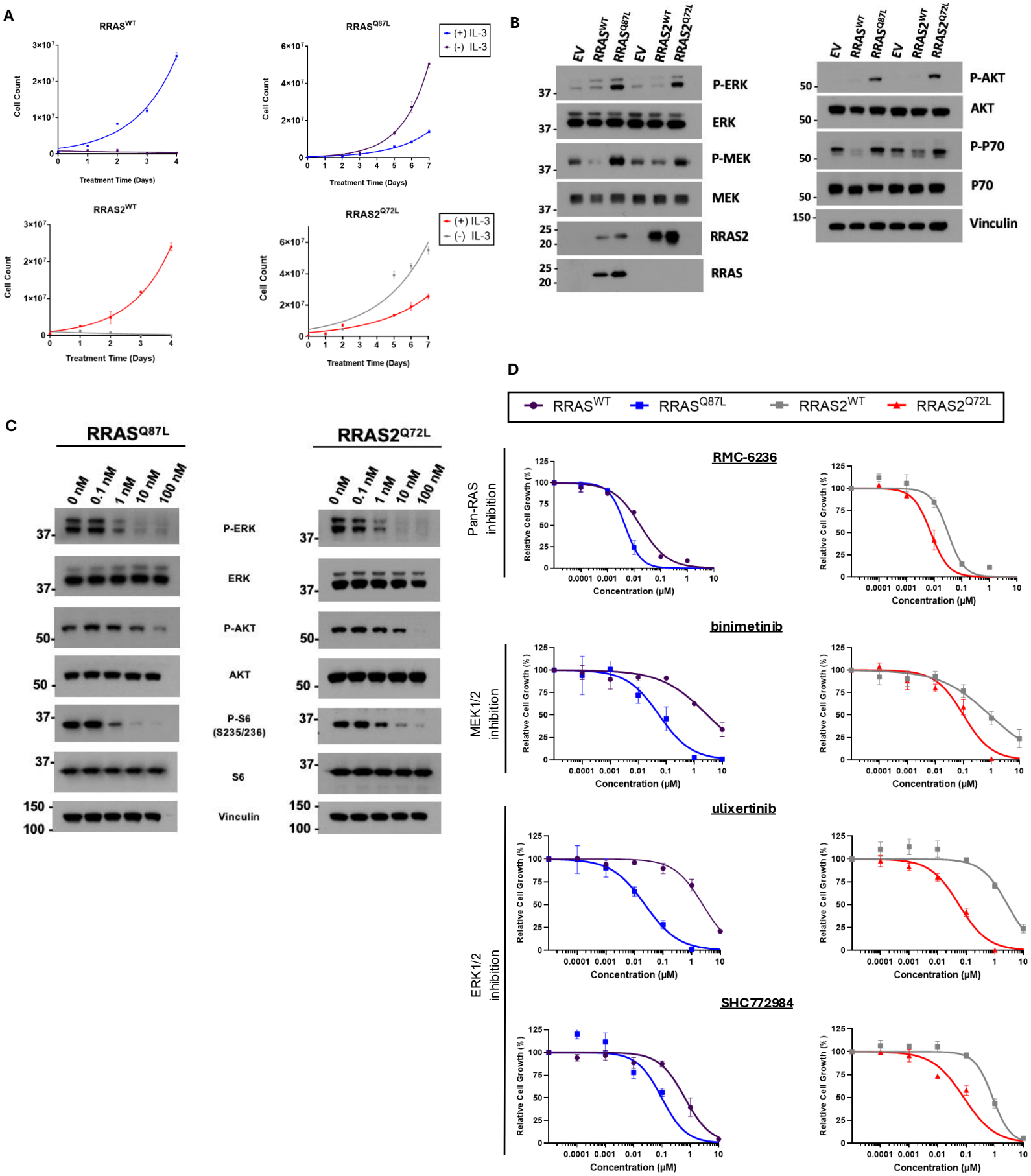
A
RRAS^WT
RRAS^Q87L
RRAS2^WT
RRAS2^Q72L
(+) IL-3
(-) IL-3
Cell Count
Treatment Time (Days)
B
EV
RRAS^WT
RRAS^Q87L
EV
RRAS2^WT
RRAS2^Q72L
P-ERK
ERK
P-MEK
MEK
RRAS2
RRAS
P-AKT
AKT
P-P70
P70
Vinculin
C
RRAS^Q87L
RRAS2^Q72L
0 nM
0.1 nM
1 nM
10 nM
100 nM
P-ERK
ERK
P-AKT
AKT
P-S6 (S235/236)
S6
Vinculin
D
RRAS^WT
RRAS^Q87L
RRAS2^WT
RRAS2^Q72L
Pan-RAS inhibition
MEK1/2 inhibition
ERK1/2 inhibition
RMC-6236
binimetinib
ulixertinib
SHC772984
Relative Cell Growth (%)
Concentration (μM)

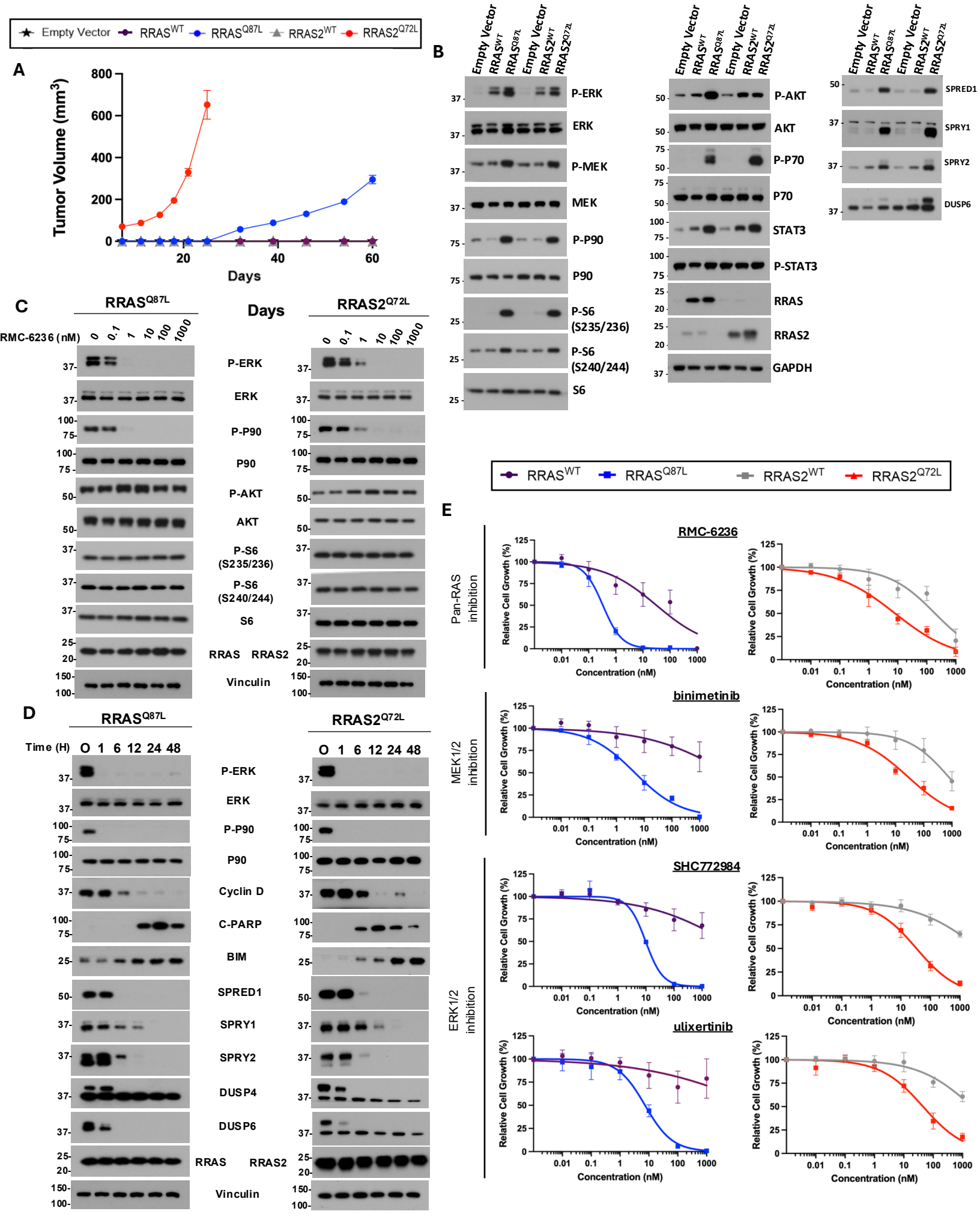
Empty Vector
RRAS^WT
RRAS^Q87L
RRAS2^WT
RRAS2^Q72L
A
Tumor Volume (mm³)
Days
B
P-ERK
ERK
P-MEK
MEK
P-P90
P90
P-S6 (S235/236)
P-S6 (S240/244)
S6
P-AKT
AKT
P-P70
P70
STAT3
P-STAT3
RRAS
RRAS2
GAPDH
SPRED1
SPRY1
SPRY2
DUSP6
C
RRAS^Q87L
RRAS2^Q72L
Days
RMC-6236 (nM)
Vinculin
D
Time (H)
Cyclin D
C-PARP
BIM
DUSP4
E
RMC-6236
binimetinib
SHC772984
ulixertinib
Pan-RAS inhibition
MEK1/2 inhibition
ERK1/2 inhibition
Relative Cell Growth (%)
Concentration (nM)

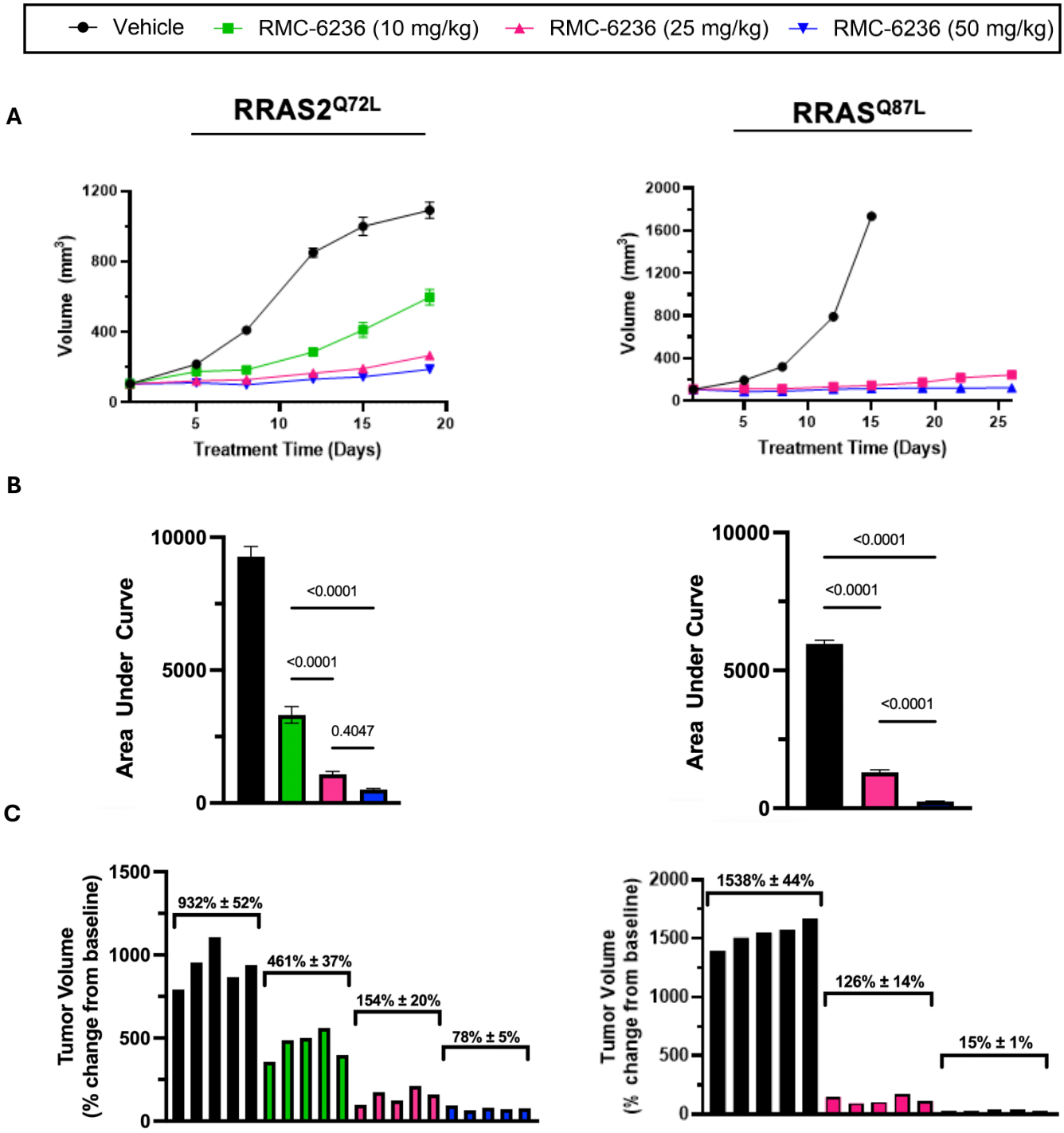
Vehicle
RMC-6236 (10 mg/kg)
RMC-6236 (25 mg/kg)
RMC-6236 (50 mg/kg)
A
RRAS2Q72L
RRASQ87L
Volume (mm3)
Treatment Time (Days)
B
Area Under Curve
<0.0001
<0.0001
0.4047
C
Tumor Volume
(% change from baseline)
932% ± 52%
461% ± 37%
154% ± 20%
78% ± 5%
1538% ± 44%
126% ± 14%
15% ± 1%